Chapter 1: Introduction

1.1 Introduction

Phosphor materials are substances that exhibit the phenomenon of luminescence, meaning they can emit light after being energized. Phosphor materials can be categorized based on their luminescent properties, excitation sources, and applications, etc. Based on luminescent properties, it is divided into two groups: fluorescent phosphors (emit light only while being excited by a light source) and phosphorescent phosphors (emit light for a period after the excitation source is removed) [4][5]. Based on excitation sources these are cathodoluminescent phosphors excited by electron beams, photoluminescent phosphors excited by photons, radioluminescent phosphors excited by radioactive decay, electroluminescent phosphors excited by an electric field, etc. They can absorb energy from various sources (e.g., ultra violet (UV) light, X-rays, electrons) and can emit light in a wide range of wavelengths, from UV to visible to infrared (IR), depending on their composition. Some phosphors are in bulk form, and some are having particle size in nano region. Based on size, dimensionality and emission properties of the phosphors materials these are integrated in many optoelectronic fields such as display technologies [6], lighting [7], medical imaging [8], security and signage [9], solar cells [10], etc.

Nanophosphor materials represent a significant advancement in the field of luminescent materials, offering enhanced performance and new functionalities that are not possible with traditional bulk phosphors [11]. Nanophosphor materials are a class of phosphor materials at the nanometer scale, typically particle size ranging from 1 to 100 nanometers. These materials exhibit unique optical properties due to their reduced dimensions and quantum

effects, making them highly attractive for advanced applications in various fields. Nanophosphors often exhibit higher brightness and more intense luminescence compared to their bulk counterparts due to their efficient light-emitting properties.

Common nanophosphor materials are zinc sulfide (ZnS), cadmium selenide (CdSe), indium phosphide (InP), zinc oxide (ZnO), halide perovskite ($CsPbX_3$, $MAPbX_3$, $FAPbX_3$: X=Cl, Br, I), fluoride ($NaYF_4$), etc. [7][12]. At the nanoscale, the optical and electronic properties of phosphors are significantly influenced by quantum confinement effects, leading to altered emission spectra and enhanced luminescence efficiency. The increased surface area relative to volume enhances the interaction of light and nanoparticles, improving performance in certain applications. The emission properties of nanophosphors can be finely tuned by controlling their size, shape, and surface chemistry.

Nanophosphor materials, with their unique quantum confinement effects and high surface-to-volume ratios, offer enhanced luminescent properties and greater tunability compared to bulk phosphors. Their unique properties and advantages open up a wide range of innovative applications, driving progress in technology and industry.

1.2 All-Inorganic Halide Perovskite

Over the past three decades, halide perovskites have revolutionized the field of perovskite applications [13]. All-inorganic cesium-lead halide perovskites ($CsPbX_3$, where X can be Cl, Br, or I) have emerged as a prominent material for photovoltaic applications due to their direct bandgap, high absorption coefficient, superior charge mobility, extended carrier lifetime, and cost-effectiveness [14]. These materials are also gaining attention for their use in color and white-light emitting diodes (LEDs) [15], fluorescence sensors [16], display technologies [17], gas sensors [18], oxygen detection sensors [19], field-effect transistors

[20], filter-free color image sensors [21], humidity sensors [22], laser fabrication [23], photodetectors [24], spectrochemical probes, explosive detectors [25], and X-ray detection [26], etc.

The origin of perovskites dates back to 1839, when the German scientist Gustav Rose discovered a new mineral composed of calcium titanate ($CaTiO_3$) during an expedition to the Ural Mountains in Russia [27]. This mineral was subsequently named "perovskite" in honor of the esteemed Russian mineralogist Lev von Perovski. Materials that share the same structural framework as $CaTiO_3$ are now referred to as perovskites. In 1958 $CsPbX_3$ halide perovskites were investigated by Møller for their photoconductivity properties [28]. These early studies marked the beginning of recognizing halide perovskites as potential semiconductor materials. Whereas, the first organic-inorganic halide perovskite, $(C_6H_5CH_2NH_3)_2PbI_4$, was reported by Dieter Weber in 1978 [29]. The pioneering work by Protesescu et al. in 2015, demonstrated the synthesis of colloidal $CsPbX_3$ nanocrystals with remarkable optical properties, such as tunable emission in the whole visible spectral region by varying the halide composition and high photoluminescence quantum yield [30].

1.2.1 Crystal Structure and Division of All-Inorganic Halide Perovskite

In recent years, a particular class of perovskites with the general formula ABX_3, where A and B represent cations and X is a halide anion, has garnered significant attention [31]. The perovskite structure, represented by the formula ABX_3, features the A cation at the corner positions, the B cation at the body center, and the X anions at the face center positions, as illustrated in Figure 1.1. In this structure, the B cation is coordinated by six X anions, forming an octahedral geometry, while the A cation is coordinated by twelve atoms

in a cuboctahedral arrangement. The structural stability of perovskites is typically described by the Goldschmidt tolerance factor, denoted as 't', which can be expressed as:

$$t = \frac{(r_A + r_X)}{\sqrt{2}(r_B + r_X)} \quad \ldots (1.1)$$

For a perovskite structure to form, the tolerance factor 't', which depends on the ionic radii r_A, r_B and, r_X is of atoms A, B, and X, respectively, should lie between 0.8 and 1.0 [32]. A tolerance factor between 0.9 and 1.0 typically results in a cubic perovskite structure, with the structure being ideally cubic t =1. When t falls within the range of 0.8 to 0.89, the perovskite structure becomes distorted, leading to possible orthorhombic, tetragonal, or rhombohedral forms. If t is less than 0.8, the B-site cation is too large, preventing the formation of a perovskite structure and favoring alternative structures like the ilmenite-type (e.g., $FeTiO_3$). Conversely, when t value exceeds 1, the B-site cation is too small, resulting in a hexagonal structure.

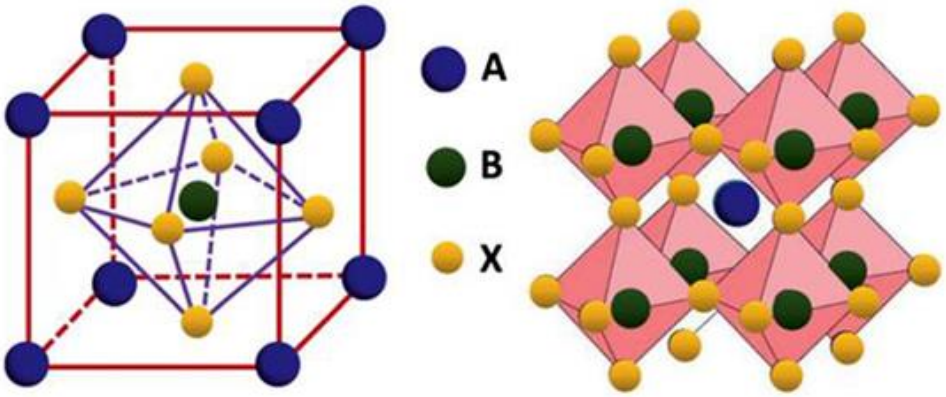

Figure 1.1: Crystal structure of perovskite with ABX_3 formula [31]**.**

In halide perovskites, the A site can be occupied by either organic cations, such as methylammonium (MA^+: $CH_3NH_3^+$) and formamidinium (FA^+: $HC(NH_2)_2^+$), or inorganic cations like cesium (Cs^+). The B site typically hosts metal cations such as Pb^{2+}, Sn^{2+}, or Ge^{2+},

while the X site is occupied by halide ions such as chloride (Cl^-), bromide (Br^-), or iodide (I^-) [33]. When an organic cation (e.g., MA^+ or FA^+) occupies the A site, the material is referred to as an organic-inorganic hybrid halide perovskite, exemplified by compounds like $MAPbX_3$ or $FAPbX_3$ [34]. Conversely, if the A site is occupied by an inorganic cation, the material is classified as an all-inorganic halide perovskite (IHP), with $CsPbX_3$ being a common example [35]. A schematic diagram in Fig. 1.2 illustrates the basic classification of perovskite based on the different types of atoms occupying the A, B, and X sites.

The halide perovskites are generally divided into two main categories: hybrid (organic-inorganic) halide perovskites and all-inorganic halide perovskites (all-IHPs), division schematic depicted in Fig. 1.2. The first organic-inorganic halide perovskite utilized for harvesting visible light was methylammonium lead iodide ($CH_3NH_3PbI_3$), reported in 2009 [36]. This material demonstrates high efficiency in photovoltaic applications, but it is hindered by poor phase stability, especially in humid conditions, and inadequate photo-stability [37]. In contrast, all-IHPs have been observed to exhibit superior stability across various environments, including humid atmospheres, light exposure, electric fields, high temperatures, and electron beam irradiation, among others [38].

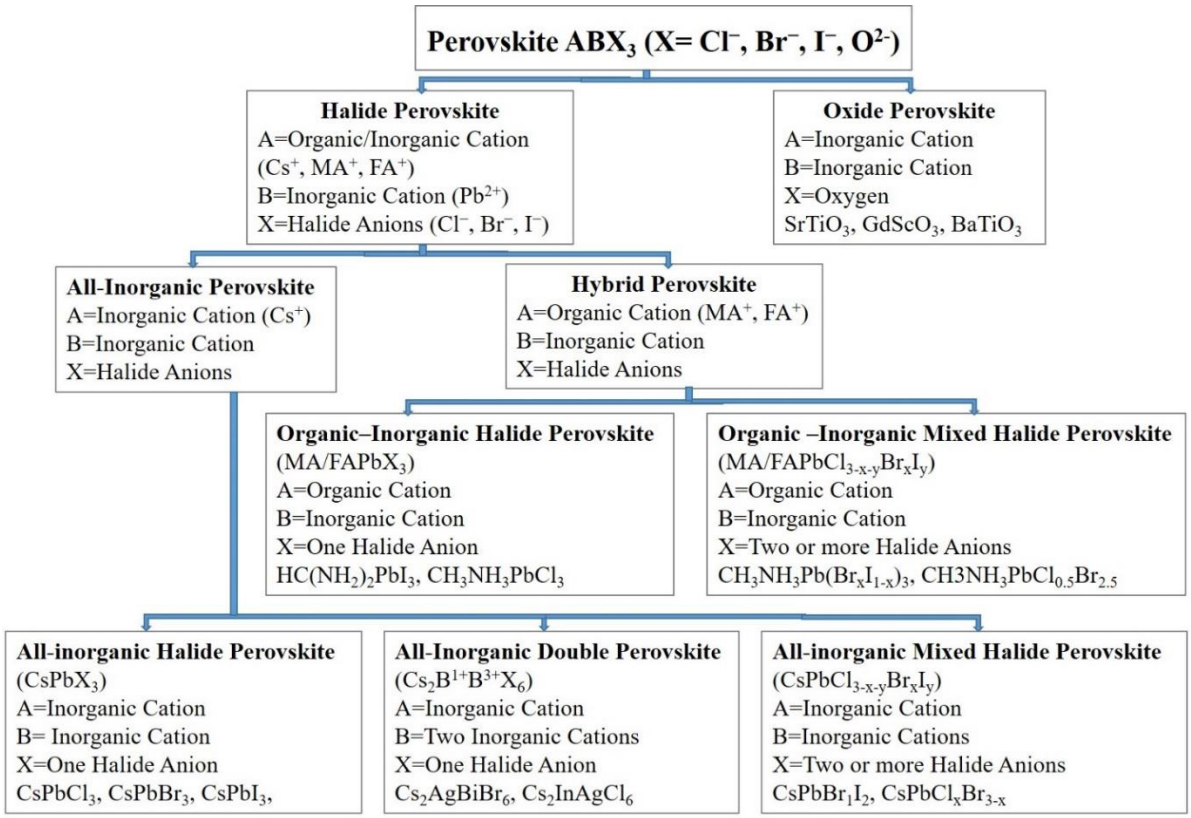

Figure 1.2: Broad classification of ABX_3 (X= Cl, Br, I, O) perovskites.

1.2.2 Optical Properties of All-Inorganic Halide Perovskite ($CsPbX_3$)

The $CsPbX_3$ (X= Cl, Br, I) show very promising optical properties such as sharp emission in the whole visible region, tunable band gap very useful for the solar cell application, high photoluminescent quantum yields (PLQYs), etc. $CsPbX_3$ have absorption in the wavelength region ranging from 390 – 680 nm and PL emission in the whole visible region from 400-700 nm [30].

The photoluminescence (PL) measurements reveal that the emission peak of $CsPbCl_3$ is centered around 410 nm, and this peak undergoes a red shift as Cl^- ions are partially or fully replaced by Br^- or I^- ions, with the PL peak for $CsPbI_3$ shifting to approximately 700 nm [39]. Figure 1.3(a) illustrates photographs of $CsPbX_3$ in hexane solution under ambient light (top) and UV-lamp illumination (bottom) [40]. The absorption and PL spectra for all- IHPs

with varying halide compositions are presented in Figure 1.3(b). These halide perovskites exhibit narrow emission peaks, with full width at half maximum (FWHM) ranging from 11 nm to 37 nm, indicating their high color purity, which is essential for various applications. Table 1.1 provides a summary of the emission peak positions, FWHM values, and PL quantum yields of $CsPbX_3$ halide perovskites with halide composition.

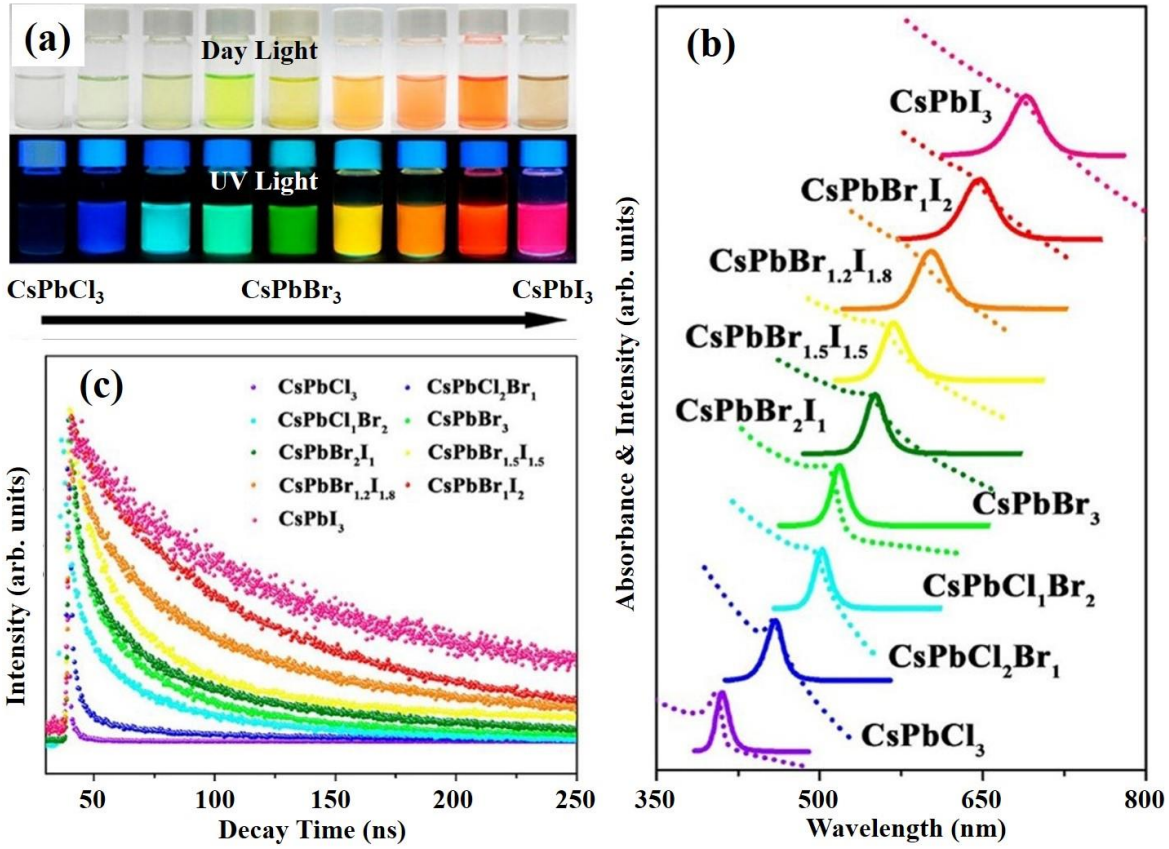

Figure 1.3*:* (a) photographs of $CsPbX_3$ in (X=Cl, Br, and I) NCs hexane solution illuminated under room light (top), and UV lamp (bottom), (b) UV-visible absorption (dotted line), and PL spectra of $CsPbX_3$, and (c) PL lifetime of $CsPbX_3$ NCs [40].

In addition to the halide composition, the size of the NCs also influences the optical properties of all- IHPs[30]. As the size of the NCs increases, the emission peak and the absorption band edge shift to longer wavelengths.

Table 1.1 PL emission properties of $CsPbX_3$ halide perovskites [41].

$CsPbX_3$	Emission Peak (nm)	FWHM (nm)	Decay Time (ns)	PLQY (%)
$CsPbCl_3$	410	11.7	1.8	26.0±0.3
$CsPbCl_2Br$	444	15.5	3.5	35.6±0.4
$CsPbCl_{1.5}Br_{1.5}$	464	16.3	8.9	61.8±0.4
$CsPbCl_1Br_2$	481	17.9	8.2	61.4±0.8
$CsPbBr_3$	520	20.3	21.1	79.8±0.9
$CsPbBr_2I_1$	587	28.2	41.1	71.2±0.5
$CsPbBr_{1.5}I_{1.5}$	631	29.4	66.2	62.7±0.2
$CsPbBr_1I_2$	660	29.9	75.0	58.5±0.7
$CsPbI_3$	700	37.0	81.1	57.5±0.4

In $CsPbX_3$ halide perovskites, the valence band maximum (VBM) originates from the antibonding interaction between Pb 6s and X np (n= 3: Cl, 4: Br, 5: I) orbitals, with the X np orbitals playing a dominant role [42][43]. Conversely, the conduction band minimum (CBM) results from the antibonding interaction between X np and Pb 6p orbitals, with the Pb 6p orbitals being the primary contributors. The A site atoms have minimal influence on both the VBM and CBM. As the atomic number of X increases from Cl to Br to I, the VBM shifts to higher energy levels, while the CBM moves to lower energy levels [43]. The bandgap of $CsPbX_3$ is inversely related to the sum of the ionic radii of the atoms involved in its formation: a smaller sum leads to greater orbital overlap and a higher bandgap. Consequently, $CsPbCl_3$ exhibits a bandgap of approximately 3.0 eV, which decreases to about 2.3 eV in $CsPbBr_3$, and reaches a lowest value of around 1.8 eV in $CsPbI_3$ [41][40].

The photoexcited exciton lifetime refers to the duration it takes for the population of electrons in a given excited state to decrease to 1/e of its initial maximum value. For $CsPbCl_3$, the radiative lifetime is relatively short and increases as the halide ion's atomic number rises, with $CsPbI_3$ exhibiting the longest radiative lifetime [44][45]. Figure 1.3(c) illustrates the variation in PL lifetime across all- IHPs with different halide compositions.

The PL decay lifetime of $CsPbX_3$ at the band-edge exciton ranges from 1.8 to 81.1 ns, measured using a pico-second pulsed laser with an excitation wavelength of 397 nm [41]. Specifically, the PL decay lifetimes for $CsPbCl_{3-x-y}Br_xI_y$ are as follows: 1.8 ns, 3.5 ns, 8.9 ns, 8.2 ns, 21.1 ns, 41.1 ns, 66.2 ns, 75.0 ns, and 81.1 ns for compositions (x, y) = (0.0, 0.0), (1.0, 0.0), (1.5, 0.0), (2.0, 0.0), (3.0, 0.0), (2.0, 1.0), (1.5, 1.5), (1.0, 2.0), and (0.0, 3.0), respectively. It is observed that perovskites with a larger bandgap, such as $CsPbCl_3$, exhibit faster decay rates compared to those with a smaller bandgap, like $CsPbI_3$ [30]. The radiative lifetime can be enhanced by mitigating thermal and concentration quenching effects.

Consequently, $CsPbX_3$ perovskites demonstrate promising optical properties that are advantageous for various optoelectronic applications, which are further explored in the following section.

1.2.3 Issues with All-Inorganic Halide Perovskites

The stability of halide perovskites can be enhanced by modifying their internal structure, specifically through adjustments to the A and B site occupied cations, halide ion compositions, dimensionality reduction, and surface modifications. Key factors influencing the structure include the Goldsmith tolerance factor "t", and the octahedral factor ($\mu = r_B/r_X$). For halide perovskites "t", between 0.8 and 0.9 typically results in a distorted perovskite structure (e.g., tetragonal or orthorhombic), while values between 0.9 and 1.0 favor the formation of a cubic structure, leading to the most stable α-phase cubic structure achieved at t = 1 [46]. Larger A-site cations tend to increase the "t" value, thereby stabilizing the perovskite structure [47][48]. Cs^+, being one of the largest inorganic cations, is often used in the synthesis of all- IHPs. However, substituting Cs^+ with organic cations can negatively impact structural stability. Within the ABX_3 perovskite structure, the B atom is located at the

center of octahedra formed by B and X atoms. The "μ" is crucial for octahedral stability, with an ideal μ value ranging from 0.414 to 0.732 [49]. This factor influences the size of the $[BX_6]^{4-}$ octahedra and the cuboctahedral voids. Therefore, the "t" and "μ" are interrelated in determining the structural stability of IHPs. Substituting smaller B site cations reduces octahedral size, increasing the "t" value and enhancing stability. Literature indicates that, at room temperature, halide perovskites with X = I, Br, and Cl show increasing stability with smaller X site ions [50]. Additionally, halide perovskites generally exhibit stability at higher temperatures, while $CsPbI_3$ shows reduced stability at low temperatures due to the tilting of $[PbI_6]^{4-}$ octahedra and the relatively large cuboctahedral voids compared to the Cs^+ cation.

The stability of all-IHPs is enhanced by incorporating various type of surface capping agents. Consequently, numerous organic compounds have been utilized to stabilize the perovskite structure [51]. In the synthesis of $CsPbX_3$ using the hot-injection method, the Cs-oleate is introduced in situ at high temperatures into an octadecene (ODE) solution containing PbI_2, oleic acid (OA), and oleylamine (OAm). The particles are stabilized by long-chain carboxylic acids and oleylammonium surface ligands [52]. In the case of $CsPbI_3$ quantum dots (QDs), ammonium ligands tend to dissociate due to weak acid-base interactions between iodide (I^-) and oleylammonium during the necessary purification processes. This loss of ligands leads to rapid agglomeration and a subsequent phase transition from the α-cubic phase to the non-perovskite δ-phase.

The stability of halide perovskites in humid environments and at elevated temperatures is a significant challenge. This stability can be enhanced through surface modifications, including the moisture-resistant layers, encapsulation, passivation, or additives [53]. For instance, phenylethylammonium chloride (PEACl), p-phenylenediammonium iodide (PPDI),

and phenylethylammonium iodide (PEAI) are commonly employed to address these issues. These additives improve the hydrophobic properties of all-IHPs, thus stabilizing the black phase perovskite structure. The hydrophobicity imparted by the alkyl chains or conjugated heterocycles in these organic cations is believed to enhance resistance to moisture [54].

In an N_2 environment, $CsPbBrI_2$ films experience a phase transition from the α-phase (black) to the δ-phase (reddish brown) due to thermal degradation. However, the incorporation of polyethyleneimine (PEI) stabilizes $CsPbBrI_2$ films during the annealing process, maintaining the α-phase. The van der Waals forces among PEI's alkyl chains increase the crystal formation energy, thus enhancing phase stability. PEI also reduces defects in all-IHPs, improving both phase and structural stability of $CsPbBrI_2$ against humidity and temperature fluctuations.

Furthermore, the use of the aromatic bi-functional ligand L-phenylalanine (L-PHE) for in-situ surface ligand management stabilizes the $CsPbI_3$ phase by coordinating with both cations and anions on the surface [55]. Additionally, the stability of $CsPbI_3$ is enhanced by using trioctylphosphine−PbI_2 (TOP−PbI_2) as a precursor [52]. The TOP-PbI_2 precursor effectively minimizes electron and hole trapping effects, which are common in phosphor materials and lead to nonradiative recombination and luminescence quenching [56].

Hence, the stability of perovskites is notably enhanced through the use of various organic surface capping agents. Additionally, the dimensionality of the perovskite structure plays a crucial role in its stability [57]. Specifically, lower-dimensional perovskites exhibit greater resistance to humidity compared to bulk 3D perovskites [58]. This indicates that reducing the dimensionality of the perovskite structure can further improve its stability.

1.2.4 Lanthanide Doping in All-Inorganic Halide Perovskites

The incorporation of Ln^{3+}-ions into $CsPbX_3$ alters its optical and optoelectronic characteristics. Substituting Pb^{2+} with smaller Ln^{3+}-ions, especially those beyond Gd^{3+}, results in lattice contraction. This substitution induces a blue shift in both the absorption edge and emission spectrum, indicating an increase in the bandgap of the Ln^{3+}-doped $CsPbX_3$ [59]. Additionally, the emission spectrum of Ln^{3+}-doped $CsPbX_3$ exhibits both the characteristic emissions of the $CsPbX_3$ matrix and those of the Ln^{3+} ions themselves, thereby extending the emission range from UV to NIR. Time-resolved spectroscopy data show that lanthanide-doped $CsPbCl_3$ has a significantly longer average lifetime compared to undoped $CsPbCl_3$, with values exceeding 1.8 ns [59]. For instance, Yb-doped $CsPbCl_3$ nanocrystals exhibit an average lifetime of 22 ns, surpassing that of the undoped material. This increased lifetime is also observed in other Ln^{3+}-doped $CsPbX_3$ variants [60]. Consequently, the doping of Ln^{3+}-ions substantially modifies the optical and optoelectronic properties of $CsPbX_3$, broadening its potential applications, which are explored in subsequent sections.

1.2.5 Applications of Lanthanide Doped All-Inorganic Halide Perovskite

Halide perovskites have gained significant attention for photovoltaic and other optoelectronic applications since their inception. Initially explored primarily for photovoltaic applications, all- IHPs are now recognized as highly versatile materials. From last few years, research has expanded to include lanthanide-doped all-IHPs due to their potential to enhance both the efficiency and stability of devices. Beyond traditional uses in photovoltaics and colored and white light-emitting diodes, lanthanide-doped all-IHPs are now being applied in emerging areas such as near-infrared (NIR) emission, NIR cameras, NIR LEDs,

luminescence-based sensing, optical encoding, and non-linear upconversion (UC) emission processes.

1.2.5.1 In photovoltaic: In the realm of photovoltaics, lanthanide-doped $CsPbX_3$ has been utilized as a layer in solar cell structures, specifically in configurations like FTO/c-TiO2/m-TiO2/Ln: $CsPbX_3$/carbon. Studies have examined the impact of doping $CsPbBr_3$ with various lanthanide ions (Sm^{3+}, Tb^{3+}, Ho^{3+}, Er^{3+}, and Yb^{3+}) on solar cell performance [61]. The results indicate that lanthanide doping significantly enhances cell performance by increasing the open-circuit voltage, improving thermal stability, and providing better resistance to humidity.

1.2.5.2 In color and white LEDs: One intriguing application of $CsPbX_3$ perovskite is their use in creating tunable colored LEDs. Recent research has also focused on lanthanide-doped all- IHPs for this purpose. For instance, doping $CsPbBr_3$ NCs with Nd^{3+} shifts the emission wavelength from 515 nm to 459 nm [62]. By encapsulating green-emitting $CsPbBr_3$ NCs and blue-emitting $CsPbBr_3$: xNd^{3+} (x = 7.2%) NCs in a poly(methyle methacrylate) (PMMA) matrix and combining them with a UV-LED that has a red-emitting $CsPbBr_{1.2}I_{1.8}$/PMMA component, WLED can be produced. This WLED exhibit an excellent color coordinate of (0.34, 0.33), a National Television System Committee (NTSC) color gamut value of 122%, and a correlated color temperature of 5310 K. Similarly, WLEDs have also been developed by integrating Yb^{3+}-doped $CsPbI_3$ with a GaN blue LED chip and a $Y_3Al_5O_{12}$: Ce^{3+} phosphor [63].

1.2.5.3 In NIR-LED and NIR camera: The all-IHPs are renowned for their distinct emissions in the visible spectrum. Incorporating lanthanide ions into these materials extends their emission into the UV and infrared regions. Specifically, Yb^{3+}-doped $CsPbBr_3$ exhibits

strong NIR emission peak at 980 nm due to the $^2F_{5/2} \rightarrow {}^2F_{7/2}$ transition in Yb^{3+} [64]. On the other hand, Yb^{3+}/Er^{3+} co-doped $CsPbCl_3$ NCs emit NIR light with a peak at 1533 nm, resulting from the $^4I_{13/2} \rightarrow {}^4I_{15/2}$ transition in Er^{3+}-ions [65]. The incorporation of Er^{3+}, Ho^{3+}, and Nd^{3+} into $CsPbCl_3$ leads to intense NIR emissions through energy transfer mediated by Mn^{2+}-ions [66]. For Er^{3+}, the emission is centered at 1542 nm from the $^4I_{13/2} \rightarrow {}^4I_{15/2}$ transition. Ho^{3+} ions produce emissions at 986 nm and 1484 nm from the $^5F_5 \rightarrow {}^5I_7$ and $^5F_5 \rightarrow {}^5I_6$ transitions, respectively. Nd^{3+}-ions give rise to three distinct emission peaks at 888, 1064, and 1339 nm, corresponding to the $^4F_{3/2} \rightarrow {}^4I_{9/2}$, $^4F_{3/2} \rightarrow {}^4I_{11/2}$, and $^4F_{3/2} \rightarrow {}^4I_{13/2}$ transitions.

The NIR cameras, which are valuable in applications such as night vision, communications, bio-imaging, and food processing, benefit from this technology. A NIR camera fabricated with Yb^{3+}-doped $CsPbCl_3$ demonstrates a peak output irradiance of 112 mW/cm^2 at 400 mA, showcasing excellent stability.

1.2.5.4 In optical thermometry: Lanthanide-doped all- IHPs exhibit a linear variation in luminescence peak intensity with changes in temperature, particularly for two thermally coupled energy levels. This property of Ln^{3+}-ions has prompted researchers to investigate their potential for non-contact temperature sensing applications. In both lanthanides and transition metals, PL intensity variations are attributed to the thermal population changes between coupled electronic states. The Ln^{3+}-ions such as Tb^{3+}, Dy^{3+}, Eu^{3+}, and Yb^{3+}, when doped into $CsPbX_3$ perovskites, have been explored for non-invasive optical thermometry.

1.2.5.5 In optical encryption and decryption: In recent years, research in optical encoding has emerged as a crucial area for detecting counterfeiting. Traditional encoding materials, which rely on limited security keys, are often vulnerable to forgery. In contrast, stimuli-

responsive luminescence materials, such as lanthanide ion-doped all-IHPs, offer enhanced optical data security. These materials exhibit luminescence emission transitions that vary based on external factors like dopant ions, temperature, and excitation energy.

For example, $CsPbBr_3$ material, applied to tracing paper with OA/OAm, can encode information [67]. The encrypted message "LZU," written using $Eu(PBA)_3AA$-$CsPbBr_3$, is only decipherable when the fluorescence of $Eu(PBA)_3AA$ is activated by NH_3 vapor. This message is doubly encrypted by temperature and pH, making it readable only under specific conditions. Additionally, optical encryption and decryption have been demonstrated using Lu^{3+}-doped $CsPbBr_3$ [68]. The message "ZJU," encoded with blue-emitting Lu^{3+}: $CsPbBr_3$ ink on white paper, remains hidden under daylight but becomes visible under UV light at 360 nm.

Thus, europium complex-decorated $CsPbBr_3$ holds promise as an advanced optical encoding material. Lanthanide doping enhances both the stability and optical characteristics of IHPs, expanding their functionality beyond conventional solar cell applications. The lanthanide ion-doped inorganic perovskites have significant potential for future applications, with ongoing theoretical and experimental research likely to uncover new uses.

1.3 Lanthanide Ions as Unique Luminescence Centers

Lanthanide ions play a crucial role in spectroscopy due to their unique electronic configurations and resulting spectroscopic properties. Lanthanide ions possess partially filled 4f orbitals that are shielded by the fully occupied 5s and 5p orbitals. [69]. This shielding effect leads to sharp and well-defined spectral lines by the f-f transition. All lanthanides have stable +3 oxidation state, however, certain lanthanides can exist in the +2 state (Eu^{2+}), either due to specific chemical environments or stabilization by ligands [70][71]. Electronic

configuration and ground energy state in stable +3 oxidation state of all the lanthanides are listed in Table 1.2.

Table 1.2: Electronic configuration, ground energy level, emission transition and peak wavelength of lanthanide.

Lanthanides Ion	Configuration	Ground State	Emission Transition
Cerium (Ce^{3+})	[Xe] $4f^1 5d^1 6s^2$	$^2F_{5/2}$	$^2D_{3/2} \rightarrow {}^2F_{5/2}$(450 nm)
Praseodymium (Pr^{3+})	[Xe] $4f^3 6s^2$	$^3H_4$	$^3P_0 \rightarrow {}^3H_4$ (480 nm)
Neodymium (Nd^{3+})	[Xe] $4f^4 6s^2$	$^4I_{9/2}$	$^4F_{3/2} \rightarrow {}^4I_{9/2}$ (880 nm)
Promethium (Pm^{3+})	[Xe] $4f^5 6s^2$	$^5H_4$	$^3P_0 \rightarrow {}^3H_4$ (485 nm)
Samarium (Sm^{3+})	[Xe] $4f^6 6s^2$	$^6H_{5/2}$	$^4G_{5/2} \rightarrow {}^6H_{7/2}$ (600 nm)
Europium (Eu^{3+})	[Xe] $4f^7 6s^2$	$^7F_0$	$^5D_0 \rightarrow {}^7F_2$ (615 nm)
Gadolinium (Gd^{3+})	[Xe] $4f^7 5d^1 6s^2$	$^8S_{7/2}$	$^6P_{3/2} \rightarrow {}^8S_{7/2}$ (400 nm)
Terbium (Tb^{3+})	[Xe] $4f^9 6s^2$	$^7D_4$	$^5D_4 \rightarrow {}^7F_5$ (543 nm)
Dysprosium (Dy^{3+})	[Xe] $4f^{10} 6s^2$	$^6H_{15/2}$	$^4F_{9/2} \rightarrow {}^6H_{13/2}$ (575 nm)
Holmium (Ho^{3+})	[Xe] $4f^{11} 6s^2$	$^5I_8$	$^5F_4 \rightarrow {}^5I_8$ (535 nm)
Erbium (Er^{3+})	[Xe] $4f^{12} 6s^2$	$^4I_{15/2}$	$^4S_{3/2} \rightarrow {}^4I_{15/2}$ (550 nm)
Thulium (Tm^{3+})	[Xe] $4f^{13} 6s^2$	$^3H_6$	$^1D_2 \rightarrow {}^3F_4$ (455 nm)
Ytterbium (Yb^{3+})	[Xe] $4f^{14} 6s^2$	$^2F_{7/2}$	$^2F_{5/2} \rightarrow {}^2F_{7/2}$ (980 nm)
Lutetium (Lu^{3+})	[Xe] $4f^{13} 5d^1 6s^2$	$^2F_{7/2}$	-

Lanthanides have sharp emission due to the Laporte forbidden f-f transition [72]. Most intense emission transition and peak wavelength is listed in Table 1.2, although most of the them show many emissions peaks mediated through the electric and magnetic dipole transitions [73][74]. The emission of the lanthanide ions spans a broad wavelengths range, including the UV, visible and near to far NIR regions. This makes them useful for different applications, from visible light emission in displays to near-infrared emission in telecommunications. Lanthanide ions often have long-lived excited states, making them useful for applications that require prolonged emission.

Lanthanide such as Tb^{3+} and Eu^{3+} can be used as a luminescent probe [75][76]. Lanthanide elements are highly suitable dopant for the phosphor materials and are used in lighting, displays, lasers, in biomedical field and in MRI (Gd^{3+}) applications. The local

environment and host matrix can slightly influence the emission spectra by causing minor shifts in the energy levels due to crystal field effects. Temperature variations can affect the intensity and width of the emission lines, typically causing broadening at higher temperatures suitable for the optical thermometry.

Hence, lanthanide ions are essential in spectroscopy due to their unique electronic structure, leading to distinctive and useful spectroscopic properties. Their sharp emission lines, long-lived excited states, and minimal environmental interference make them invaluable in various scientific and industrial applications, from fluorescence spectroscopy to optical amplification and imaging.

1.3.1 Spectroscopy of Eu^{2+}/ Eu^{3+}-ion

Europium primarily exists in two oxidation states: Eu^{2+} and Eu^{3+}. Eu^{2+} ions typically exhibit a characteristic blue emission, while Eu^{3+} ions emit prominent red light [77]. This dual oxidation state behavior is relatively rare and contributes to europium's unique spectroscopic characteristics. The emission spectrum of Eu^{2+} is dominated by broad bands due to transitions between $4f^6 5d^1$ and $4f^7$ electronic states [78][79]. These transitions are allowed, resulting in strong and intense luminescence. There are many excitation transitions from the ground energy level $^7F_0$ to the various higher energy levels [77]. Although a few excitation transition are arise from the $^7F_2$ and $^7F_2$ levels also and are depicted in energy level diagram of Eu^{3+}-ion in chapter 5. All these transitions are listed in Table 1.3. On the other hand, Eu^{3+} ions show sharp emission lines due to transitions within the 4f orbitals, which are partially shielded from the environment by outer electrons. The prominent transitions are from the excited state $^5D_0$ to the ^7F_J (J = 0, 1, 2 ,3, 4), with $^5D_0 \rightarrow {}^7F_2$ being the most intense transition and responsible for the red (615 nm) emission. A few emission transitions are

observed from the $^5D_1$ level also. All the emission transitions and corresponding wavelength of Eu^{3+} are listed in Table 1.4.

Table 1.3: Excitation transitions of Eu^{3+}-ion and their corresponding peak wavelength.

Excitation Transition	Wavelength (nm)
$^7F_0 \rightarrow {}^5H_3$	326
$^7F_0 \rightarrow {}^5D_4$	361
$^7F_1 \rightarrow {}^5D_4$	366
$^7F_0 \rightarrow {}^5G_3$	374
$^7F_0 \rightarrow {}^5G_2$	380
$^7F_0 \rightarrow {}^5L_7$	386
$^7F_0 \rightarrow {}^5L_6$	395
$^7F_0 \rightarrow {}^5D_3$	415
$^7F_0 \rightarrow {}^5D_2$	464
$^7F_0 \rightarrow {}^5D_1$	525
$^7F_1 \rightarrow {}^5D_1$	536
$^7F_2 \rightarrow {}^5D_1$	555
$^7F_0 \rightarrow {}^5D_0$	589
$^7F_1 \rightarrow {}^5D_0$	591

Table 1.4: Emission transitions of Eu^{3+}-ion and their corresponding peak wavelength.

Emission Transition	Wavelength (nm)
$^5D_1 \rightarrow {}^7F_1$	537
$^5D_1 \rightarrow {}^7F_2$	555
$^5D_0 \rightarrow {}^7F_0$	583
$^5D_0 \rightarrow {}^7F_1$	593
$^5D_0 \rightarrow {}^7F_2$	615
$^5D_0 \rightarrow {}^7F_3$	650
$^5D_0 \rightarrow {}^7F_4$	690

Energy transfer processes involving europium ions are crucial in designing efficient phosphors. For instance, in many commercial phosphors, energy is transferred from a host lattice or a sensitizer to the europium ion, enhancing the overall emission efficiency. This is evidenced by the experimental observations discussed in Chapter 5.

The formation of a charge transfers band (CTB) involving europium is an important aspect of its spectroscopic properties, particularly in the context of luminescent materials and phosphors. CTBs are typically associated with the movement of an electron from one ion or

ligand to another within a complex. In Eu^{3+} CTB involves the transfer of an electron from a ligand orbital (often a non-bonding oxygen orbital in oxides) to the empty 4f or 5d orbitals of Eu^{3+}-ion [80]. Charge transfer bands are typically broad in comparison to the sharp f-f transitions of Eu^{3+}. This is because the charge transfer involves a significant change in the electronic environment. The exact position of the CTB depends on the nature of the ligands and the host matrix. For europium in oxide materials, the CTB usually appears in the UV region, often around 250-350 nm.

The emission spectra of Eu^{3+} (magnetic dipole transitions)/Eu^{2+} (f-d transitions) ions are highly sensitive to their chemical environment. This makes europium a useful probe for studying the local environment in various materials, as changes in the symmetry or composition of the surrounding matrix can significantly affect the spectral characteristics.

1.3.2 Spectroscopy of Tb^{3+}-ion

Terbium (Tb) has the electronic configuration $[Xe]4f^{9}6s^{2}$. Like other lanthanides, the 4f electrons are partially shielded by the outer 5s and 5p electrons, which makes the 4f-4f transitions relatively less affected by the surrounding environment. Although, the valence state of Tb is most commonly +3 in its compounds. The Tb can also exist in the +4 oxidation state (Tb^{4+}), but this is much less common and typically occurs in specific compounds, such as TbO_2 [81]. However, Tb^{3+} is by far the dominant and most stable valence state of terbium in both inorganic and organometallic compounds.

The excitation transitions of Tb^{3+}-ion are primarily within the UV and blue regions. In UV-region one excitation transition is from $^{7}F_{6} \rightarrow {}^{5}G_{6}$ with peak at around 280 nm. Second excitation transition in the UV region in this range 350-360 nm from $^{7}F_{6} \rightarrow {}^{5}D_{3}$, efficiently leads to the population of the higher energy levels, which subsequently decay to the

$^5D_4$ level, producing the strong green emission at 543 nm. The blue excitation transition peak at 480 nm is from $^7F_6 \rightarrow {}^5D_3$. This is the direct excitation transition to populate the $^5D_4$ level that given intense green emission. Tb exhibits characteristic green emission lines when doped in phosphor material, particularly around 543 nm, from to the $^5D_4 \rightarrow {}^7F_5$ transition under UV excitation. Although it shows other emission transitions in the visible region. These are 488, 581 and 620 nm, which arise from the $^5D_4$ to the different J value of ^7F_J in Tb^{3+}-ion [82][83]. The 488 nm is due to the transition from the $^5D_4 \rightarrow {}^7F_6$, 543 nm peak ascribed to $^5D_4 \rightarrow {}^7F_5$, 581 nm to the $^5D_4 \rightarrow {}^7F_4$, and 620 nm to the $^5D_4 \rightarrow {}^7F_3$. This green fluorescence is one of the most notable features of Tb^{3+} and is utilized in various applications like phosphors and fluorescent materials. Tb^{3+} containing phosphor material can be used for fluorescent Lamps and LEDs, Security Inks, in display technologies to enhance color rendering and efficiency, in optical data storage due to its magneto-optical properties.

1.3.3 Upconversion Mechanism in Er^{3+}/ Yb^{3+}-ions Pair

Upconversion (UC) is a nonlinear optical phenomenon in which two or more low-energy photons are absorbed sequentially, resulting in the emission of a photon with higher energy [84][85]. This process is especially prominent in certain rare-earth ions like erbium (Er^{3+}) and ytterbium (Yb^{3+}), which are commonly used in UC materials. The interaction between these ions can significantly enhance the UC efficiency due to their favorable energy levels and efficient energy transfer mechanisms.

Mechanism:

UC mechanism in Er^{3+}/ Yb^{3+}-ions pair can be understood by the following steps [86][87];

(i) Energy Levels involve in UC: Er^{3+} ions have multiple energy levels that can be utilized for UC, notably the levels corresponding to $^4I_{15/2}$ (ground energy level), $^4I_{13/2}$, $^4I_{11/2}$, $^4I_{9/2}$, $^4F_{9/2}$, $^4S_{3/2}$, $^2H_{11/2}$, $^4F_{7/2}$, $^2H_{9/2}$, and $^4G_{11/2}$ depicted in Fig. 1.4. Yb^{3+} ion primarily have two energy levels involved in the UC process: the $^2F_{7/2}$ (ground energy level) and the $^2F_{5/2}$ (higher energy level).

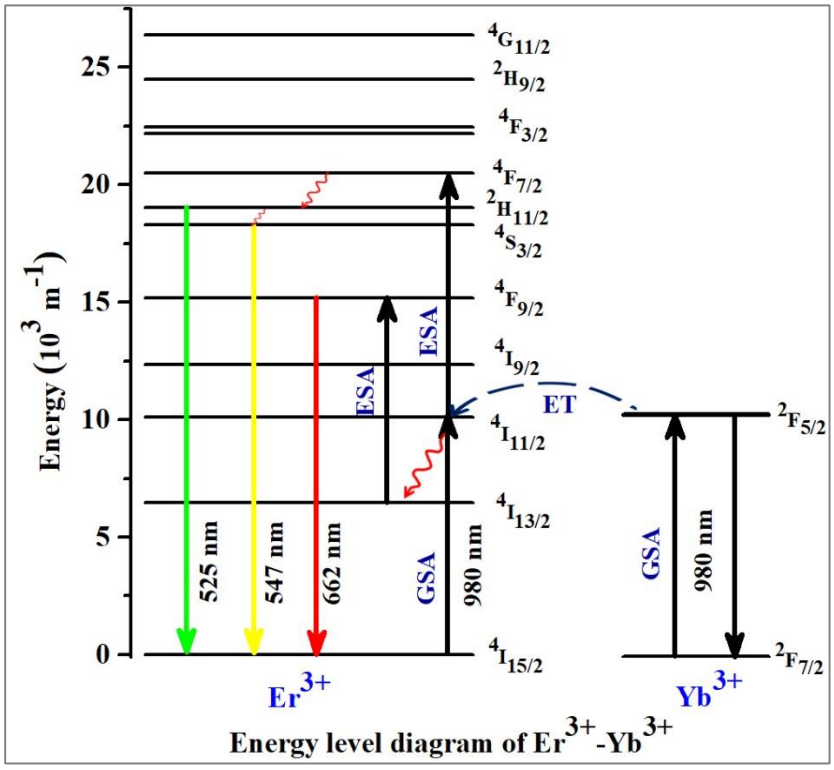

Figure 1.4: Energy level diagram of Er^{3+}/ Yb^{3+} involve in UC mechanism.

(ii) Absorption and Energy Transfer: Yb^{3+} ions act as sensitizers due to their large absorption cross-section for NIR photon, typically around 980 nm. Upon absorbing NIR photons, the ions goes from the $^2F_{7/2}$ to the $^2F_{5/2}$ level of Yb^{3+}. The excited Yb^{3+} ion transfers its energy non-radiatively to a neighboring Er^{3+} ion. This process can be described as:

$$Yb^{3+}\ (^2F_{5/2}) + Er^{3+}\ (^4I_{15/2}) \rightarrow Yb^{3+}\ (^2F_{7/2}) + Er^{3+}\ (^4I_{11/2})$$

This transfers the Er^{3+} ion from its ground level $^4I_{15/2}$ to the to an intermediate level $^4I_{11/2}$.

(iii) Sequential Photons Absorption: The Er^{3+} ion in the $^4I_{11/2}$ level can absorb another NIR photon either directly or through energy transfer from another excited Yb^{3+} ion, leading to a higher level like $^4F_{7/2}$. This sequential absorption can proceed through various intermediate states, leading to the population of higher energy levels like $^4F_{9/2}$, $^4S_{3/2}$, and $^2H_{11/2}$.

(iv) Radiative Emission: From the higher excited level, the Er^{3+} ion can relax back to lower energy states through radiative emission, resulting in UC visible or ultraviolet light. For example: transitions from $^2H_{11/2}$ and $^4S_{3/2}$ levels result in green emission ~525 nm and ~547 nm, respectively. Similarly transition from $^4F_{9/2}$ to $^4I_{15/2}$ give red emission at ~660 nm.

Hence, the synergy between Yb^{3+} and Er^{3+} ions, with Yb^{3+} serving as an efficient sensitizer and Er^{3+} as the emitter, makes the Yb^{3+}/Er^{3+} co-doped systems highly effective for UC applications, such as in bioimaging, photovoltaics, solid-state lasers, optical thermometry, and other optoelectronic applications. Other lanthanides pairs used to achieve the UC are thulium (Tm^{3+}) and ytterbium (Yb^{3+}) emits in the blue region, holmium (Ho^{3+}) and ytterbium (Yb^{3+}) emits green and red.

Advantages of UC emission is that the materials excited by lower-energy photons experience less photobleaching compared to those excited by higher-energy photons. Infrared light used in bioimaging can penetrate deeper into biological tissues compared to visible light. Low Background Interference: At the same time, the use of near-infrared excitation minimizes interference from autofluorescence in biological samples. Since, upconversion is a non-linear process, obviously, lasers are required for the excitation purpose.

1.4 Metal Organic Frameworks

Metal-Organic Frameworks (MOFs) possess unique spectroscopic properties due to their hybrid nature, combining metal ions or clusters with organic linkers. These properties are significant for various applications, including catalysis, sensing, gas storage, and separation, etc. [88]. The synthesis of MOFs generally involves the self-assembly of metal ions with organic linkers through coordination bonds [89]. Common methods of synthesis include: solvothermal, hydrothermal, microwave-assisted synthesis, etc. [90]. Linkers with extended π-conjugation, such as terephthalic acid or bipyridine derivatives, can absorb light efficiently and transfer energy to the metal centers. This can result in strong luminescence due to enhanced excitation. Introducing functional groups (e.g., $-NH_2$, -OH, -COOH) on the linkers can alter the electronic properties and, consequently, the luminescence behavior. Linkers designed with donor-acceptor interactions can facilitate charge transfer processes that affect luminescence. For example, a linker with electron-donating and electron-withdrawing groups can create intramolecular charge transfer states that lead to unique luminescence properties.

MOFs exhibit various electronic transitions in the UV-Vis region, attributable to the metal ions and the organic linkers [91]. Also, many MOFs show metal-to-ligand charge transfer (MLCT) or ligand-to-metal charge transfer (LMCT) bands, which are critical for understanding their electronic structure, optical and catalytic properties.

MOF exhibits luminescence from the various luminescent centers. Some MOFs exhibit luminescence originating from the metal centers, particularly those containing transition metals or lanthanides known as metal-centered emission [91]. Specialty of the lanthanide based MOFs are discussed in subsequent section. Organic linkers can also contribute to luminescence, especially if they contain conjugated systems termed as linker-centered

emission. The luminescence properties can be tuned by selecting different metal ions or organic linkers, as well as by incorporating guest molecules/compounds within the pores of MOFs. If guest molecule is a phosphor material such as perovskite, then it also exhibits its own characteristic peak in the emission spectrum called the guest-centered emission. Energy transfer between the metal centers and organic linkers can enhance the overall luminescence efficiency.

1.4.1 Lanthanide Metal Organic Frameworks

Lanthanide Metal-Organic Frameworks (Ln-MOFs) are a fascinating class of materials that combine the unique properties of lanthanide ions with the versatile structures of MOFs [92]. These materials have garnered significant attention due to their potential applications in various fields such as luminescence [93], catalysis [94], gas storage [95], sensing [96], and drug delivery [97], etc. Lanthanide ions (e.g., Eu^{3+}, Tb^{3+}, Dy^{3+}) exhibit sharp emission bands and long luminescence lifetimes, making Ln-MOFs excellent candidates for applications in lighting [93] and bio-imaging [98]. These materials can be tailored to emit in specific parts of the spectrum, from ultraviolet to near-infrared. Ln-MOFs can be constructed from a variety of organic linkers and lanthanide ions, leading to a wide range of structures with different pore sizes and shapes [99]. The coordination environment of lanthanide ions allows for various geometries, contributing to the diversity of the resulting frameworks. Lanthanide ions exhibit sharp, well-defined emission lines due to 4f-4f electronic transitions, which are minimally affected by the surrounding environment. The f-f transitions are Laporte-forbidden, resulting in weak absorption bands. However, this can be enhanced by organic linkers or antenna effect. The organic linkers in MOFs can absorb over a broad range of wavelengths, transferring energy efficiently to the lanthanide centers. By selecting different

lanthanide ions (e.g., Eu^{3+} for red, Tb^{3+} for green, Tm^{3+} for blue), Ln-MOFs can emit various colors, useful in multiplexed sensing and imaging. In a MOF incorporating Eu^{3+} ions, thenoyltrifluoroacetone (TTA) as a sensitizing ligand, and phenanthroline (Phen) as an ancillary ligand, the TTA ligand absorbs UV light and transfers the energy to Eu^{3+}, which then emits red light. Changing the lanthanide ion (e.g., to Tb^{3+}) results in green emission.

Incorporating multiple lanthanide ions into a single MOF structure can result in dual or multiple emissions, enabling ratiometric sensing. Ln-MOFs exhibit high resistance to photobleaching compared to organic dyes, making them suitable for prolonged exposure in sensing and imaging applications. Introducing functional groups to the organic linkers or modifying the lanthanide coordination environment can further enhance the properties and functionalities of Ln-MOFs.

In conclusion, Ln-MOFs represent a versatile and promising area of materials science, with ongoing research aimed at overcoming current challenges and exploring new applications.

1.4.2 Inorganic Halide Perovskite Encapsulated with Metal Organic Framework

In Ln-MOFs, the luminescence emission is from the metal center i.e., Ln^{3+}-ion, and/or from the organic linker-centered emission. If, Ln-MOFs contains phosphor molecule as a guest then additional emission from the guest center is also observed in the emission spectrum [91]. Incorporating guest molecules such as small organic dyes, metal complexes, or even gases into the pores of MOFs can modify the local environment of the luminescent centers along with the guest molecule. The interaction between the MOF and guest molecules can result in energy transfer processes or changes in the electronic structure of the MOF. For

instance, encapsulated fluorescent dyes can transfer energy to the MOF framework or vice versa, altering the overall luminescence. Guest emission can also be tuned.

Halide perovskite such as $MAPbX_3$, $FAPbX_3$ and $CsPbX_3$ as a guest centered emission in MOFs have been reported [91][99]. However, stability issue in organic inorganic halide perovskite is more compared to the inorganic one. The inorganic halide perovskite ($CsPbX_3$, X=Cl, Br, I) is one of the suitable guest molecule for the guest centered emission in Ln-MOFs due to its extra-ordinary properties such as sharp and tunable emission in the whole visible region through the halide (X=Cl, Br, I) compositional mapping. Many reports on Ln-MOFs such as Eu-MOFs, Tb-MOFs with various organic linker are also available.

Eu-MOFs shows characteristic emission peaks of Eu^{3+}-ion at 583, 593, 615, 650, and 690 nm which arise from the transitions from $^5D_0$ to the ^7F_J (J = 0, 1, 2 ,3, 4) [100][101]. Encapsulating $CsPbX_3$ into the Eu-MOFs, reveal one extra emission peak of $CsPbX_3$. Similarly, Tb-MOFs consist of peaks at 488, 581 and 620 nm in the emission spectrum that arise from the excited level $^5D_4$ to the different J values of ^7F_J in Tb^{3+}-ion [102]. The $CsPbX_3$ incorporation with Tb-MOFs integrate additional peak of $CsPbX_3$ in emission profile. Since, emission peak of $CsPbX_3$ depends on the halide ion present, its emission can be tuned in whole visible range by halide compositional mapping on our application choice. Also, halide perovskite emission depends on the particle size of $CsPbX_3$. So, $CsPbX_3$ offer bidirectional way to control the emission of guest center in the Ln-MOFs.

Hence, by carefully selecting the metal ions, organic linkers, and guest molecules, researchers can design MOFs with tailored luminescence properties. These adjustments allow for the creation of materials with specific emission wavelengths, enhanced luminescence

efficiencies, and responsive behaviors suitable for a wide range of applications, including sensing, imaging, and photonics.

1.5 Scandate Oxide Perovskite

From a spectroscopic point of view, scandate materials, particularly rare earth scandates such as lanthanum scandate ($LaScO_3$), gadolinium scandate ($GdScO_3$), and others, exhibit unique properties that are of significant interest [103]. The scandate materials typically have wide bandgaps. For example, $LaScO_3$ and $GdScO_3$ have bandgaps in the range of 5.5-6 eV [104][105]. The wide bandgap results in transparency in the visible to near-ultraviolet region, making these materials suitable for optical applications where high transparency is required. $LaScO_3$ typically crystallizes in an orthorhombic perovskite structure [104]. $GdScO_3$ also adopts an orthorhombic perovskite structure. Lanthanide based scandate oxide perovskite have high dielectric constant in the range (20-30). High dielectric constant, making them suitable for use in capacitors with high energy storage capacity and as gate dielectrics in field-effect transistors (FETs). Its high dielectric constant helps to reduce leakage currents and improve the performance of metal-oxide-semiconductor field-effect transistors (MOSFETs). Dielectric loss of the scandate is very low, which is crucial for minimizing energy dissipation in electronic devices. Along with these advantageous electric properties, it has high melting points and excellent thermal stability, allowing their use in high-temperature environments.

$GdScO_3$ is an intriguing material with a variety of optoelectronic properties that make it valuable for advanced applications in electronics and optics. $GdScO_3$ has a wide bandgap of approximately 5.8 eV [106]. This makes it an excellent insulator and transparent material in the visible and ultraviolet (UV) regions. $GdScO_3$ has a relatively high refractive index, which

is beneficial for optical waveguides and other photonic applications. The wide bandgap also reduces the likelihood of thermal excitation of charge carriers, enhancing its stability and performance in optoelectronic applications.

Hence, lanthanide based scandate perovskite materials are integral to advancing modern technology due to their diverse and advantageous optoelectronic properties. Their applications span across electronics, optoelectronics, high-temperature environments, and research. The unique combination of high dielectric constants, thermal stability, and optical properties makes them highly sought after in various cutting-edge fields.

1.5.2 Lanthanide Doped Scandate Oxide Perovskite

Rare earth scandates can be doped with other rare earth ions (such as Tm^{3+}, Ho^{3+}, Eu^{3+}, Tb^{3+}, Dy^{3+}, Er^{3+}, and Yb^{3+}) to create materials with specific photo-luminescent properties [107][108]. This lanthanide doped scandates exhibit strong luminescence due to Laporte forbidden f-f transitions. The photoluminescence spectra typically show sharp emission lines corresponding to the electronic transitions of the dopant ions, superimposed on the broad bandgap luminescence of the host material.

The Er^{3+}, Yb^{3+}-doped $GdScO_3$ exhibits excellent UC luminescence properties, making it a versatile material for various advanced applications [109]. The efficient energy transfers between Yb^{3+} and Er^{3+} ions (detailed discussion is given in section 1.3.3), combined with the favorable host lattice properties of $GdScO_3$, results in strong and stable UC luminescence.

Optical thermometry based on combined Er^{3+}, Yb^{3+}- doped $GdScO_3$ leverages the temperature-dependent luminescence properties of these dopant ions. The principle of optical thermometry often relies on the luminescence intensity ratio of two emission bands from dopant ions (e.g., Er^{3+} and Yb^{3+}). The relative intensities of these emissions change with

temperature, allowing for accurate temperature measurements. Er^{3+}, Yb^{3+}-doped $GdScO_3$ can capable of functioning across a broad temperature range, making it adaptable for diverse applications, from low-temperature biological systems to high-temperature industrial processes. Optical thermometry using luminescence is a non-contact method, which is particularly advantageous for measuring temperatures in sensitive or inaccessible areas.

1.5.1 Stability and Application of Scandate Oxide Perovskite

Stability of the lanthanide based scandate oxide perovskite is relatively high compared to the halide perovskite. It retains in luminescence properties very long time. High melting points and excellent thermal stability, allowing their use in high-temperature environments for e.g. optical thermometry. Good mechanical strength and hardness, which can be advantageous in structural applications. $GdScO_3$ has relatively low phonon energy, which suppresses non-radiative relaxation process and enhances UC emission efficiency when it is doped with lanthanide ions upconversion pair such as Er^{3+} and Yb^{3+}. Transparent in the visible and NIR regions, making them suitable for optical applications.

1.6 Objectives and Motivation

Inorganic halide perovskites, which are comparatively more stable than the organic-inorganic halide perovskites, possess promising optoelectronic properties and can be explored for various applications. Although, as discussed above, stability issue is the one of the important concern for the researchers and scientific groups. To increase the stability, various metal ions are doped into it. Also, this is interfaced with other host material to form complex or encapsulated into the void of the host matrix. Interaction between the doped metal ion or other matrix with the inorganic halide perovskites reflect peculiar properties. Therefore, the research objective is to address the followings;

- Increase the stability of all-inorganic halide perovskites.
- The study of the optical properties due to Ln^{3+}-ion doping.
- Interaction of all-inorganic halide perovskites with other matrices such as metal organic frameworks.
- To enhance the stability and properties of all-inorganic halide perovskite by encapsulating all-inorganic halide perovskites into metal organic framework.
- To study the energy transfer mechanism among lanthanide ions, and host matrix.
- Suitability of the material for optical applications such as optical encryption-decryption, and white LEDs.
- To study photon upconversion and thereby thermometry study in scandate oxide perovskite.

To address above mentioned points, inorganic halide perovskite ($CsPbBr_3$) nanocrystal is synthesized by hot-injection method. Further, in this host Eu^{2+}-ions are doped. Eu-MOF as well as Tb/Eu-MOF is synthesized using hydrothermal method and used to encapsulate IHPs. The study has been extended by encapsulating $CsPbBr_3$ and $CsPbCl_{1.5}Br_{1.5}$, respectively, in Eu-MOF and Tb/Eu-MOF. In the last, Er^{3+}, Yb^{3+}-doped $GdScO_3$ is synthesized using self-propagated gel-combustion method.

The precise objectives and motivations of the thesis work are as follows;

(1) To address the stability and optical properties, and energy transfer path, $CsPbBr_3$ and Eu-doped $CsPbBr_3$ NCs are synthesized via hot-injection method.

(2) Study the properties change after the doping of Eu^{2+}-ion into $CsPbBr_3$ NCs.

(3) Stability enhancement of inorganic halide perovskites by interfaced with lanthanide metal-organic frameworks synthesized by hydrothermal method.

(4) Study of $CsPbBr_3$@ Eu-MOF color tunable emission behavior, energy transfer between $CsPbBr_3$ and Eu-MOF, and applicability for advanced anti-counterfeiting application.

(5) Morphology study and tuning the emission intensity of Tb^{3+}-ion in Tb/Eu-MOF synthesized via hydrothermal synthesis route.

(6) To study the energy-transfer scheme among $CsPbCl_{1.5}Br_{1.5}$, Tb^{3+} and Eu^{3+}-ions and suitability of $CsPbCl_{1.5}Br_{1.5}$@Tb/Eu-MOF for the WLED application.

(7) Upconversion and optical thermometry study in Er^{3+}, Yb^{3+}-doped $GdScO_3$ synthesized using self-propagated gel-combustion method.

The detailed procedure of each synthesis techniques, characterization, and methods used for the analysis of obtained data is discussed in Chapter 2. Whereas, the findings of the each synthesized samples are elaborated each separately in subsequent Chapters.